JACS
JOURNAL OF THE AMERICAN CHEMICAL SOCIETY

COMMUNICATION

pubs.acs.org/JACS

Characterization of a High-Spin Non-Heme Fe^{III}—OOH Intermediate and Its Quantitative Conversion to an Fe^{IV}=O Complex

Feifei Li,[†] Katlyn K. Meier,[‡] Matthew A. Cranswick,[†] Mrinmoy Chakrabarti,[‡] Katherine M. Van Heuvelen,[†] Eckard Münck,*[,‡] and Lawrence Que, Jr.*[,†]

[†]Department of Chemistry and Center for Metals in Biocatalysis, University of Minnesota, Minneapolis, Minnesota 55455, United States

[‡]Department of Chemistry, Carnegie Mellon University, Pittsburgh, Pennsylvania 15213, United States

Supporting Information

ABSTRACT: We have generated a high-spin Fe^{III}—OOH complex supported by tetramethylcyclam via protonation of its conjugate base and characterized it in detail using various spectroscopic methods. This Fe^{III}—OOH species can be converted quantitatively to an Fe^{IV}=O complex via O—O bond cleavage; this is the first example of such a conversion. This conversion is promoted by two factors: the strong Fe^{III}—OOH bond, which inhibits Fe—O bond lysis, and the addition of protons, which facilitates O—O bond cleavage. This example provides a synthetic precedent for how O—O bond cleavage of high-spin Fe^{III}—peroxo intermediates of non-heme iron enzymes may be promoted.

Cleavage of the O—O bond of Fe^{III}—OOH species is a key step in the O_2 activation mechanisms of cytochrome P450,[1] Rieske dioxygenases,[2] and even methane monooxygenase (MMO),[3] leading to high-valent iron—oxo species that effect organic substrate oxidation. On the other hand, Fe—O bond cleavage to release H_2O_2 must occur in the catalytic cycle of superoxide reductase (SOR)[4] and for cytochrome P450 reactions that exhibit uncoupling.[1] While protonation of the proximal O atom of the Fe^{III}—OOH unit can be readily envisioned as the step needed to release H_2O_2, the mechanism for O—O bond cleavage is not as simple. For heme peroxidases and cytochrome P450, it is generally accepted that protonation of the distal O atom of the low-spin Fe^{III}—OOH intermediate facilitates the heterolysis of the O—O bond.[1] This notion should also apply to non-heme iron systems, but the likely *high-spin* state of iron—peroxo species in non-heme enzymes could raise the barrier for O—O bond lysis relative to that for *low-spin* counterparts in heme enzymes.[5] The scarcity of experimental evidence further limits insights into O—O bond scission by non-heme enzymes. The only mechanistically relevant information available is for MMO, where the conversion of the peroxodiiron(III) intermediate to the diiron(IV) oxidant exhibits a pH dependence and a H/D solvent kinetic isotope effect,[3] emphasizing the key role played by a proton in O—O bond cleavage. Among synthetic complexes, there are only a few non-heme Fe^{III}—OOH complexes that have been spectroscopically well-characterized,[6,7] but none of them has been directly observed to generate a high-valent iron—oxo intermediate, thus making it difficult to obtain mechanistic insights into this key step in iron-catalyzed oxygen activation.

To obtain the first example of an Fe^{III}—OOH complex that can undergo O—O bond cleavage to generate a high-valent iron—oxo complex, we focused on trapping of $[Fe^{III}(TMC)(OOH)]^{2+}$ (**2**) (TMC = tetramethylcyclam; see Scheme 1A for its structure), a yet-elusive species invoked in reactions of O_2 with $[Fe^{II}(TMC)(CH_3CN)]^{2+}$ that afford $[Fe^{IV}(O)(TMC)(CH_3CN)]^{2+}$ (**3**) in 60—80% yield as the final product.[8] Herein we report the high-yield generation of **2** by protonation of the previously reported $[Fe^{III}(TMC)(O_2)]^{+}$ complex (**1**)[9] at −40 °C, its detailed spectroscopic characterization, and kinetic studies that shed mechanistic light on the quantitative conversion of **2** to **3** (Scheme 1B).

Complex **1** was generated using the published procedure[7] by treating 2.0 mM $[Fe^{II}(TMC)(CH_3CN)]^{2+}$ in CH_3CN with 10 equiv of NEt_3 followed by 20 equiv of H_2O_2 in CH_3CN at −40 °C. Complex **1** exhibits a λ_{max} of 835 nm (Figure 1 left) with an ε value of 650 M^{-1} cm^{-1}, as established with the aid of Mössbauer data (see below). Upon addition of 20 equiv of $HClO_4$ at −40 °C, **1** was converted immediately to a short-lived ($t_{1/2} \sim 1$ min) maroon intermediate (**2**) with a shoulderlike absorption feature at ∼500 nm ($\varepsilon = 450$ M^{-1} cm^{-1}), which in turn decayed to give the signature absorption feature of **3** (Figure 1 right). The significant blue shift observed in the conversion of **1** to **2** was noted previously in the protonation of other non-heme $Fe^{III}(\eta^2\text{-}O_2)$ species, consistent with the weaker basicity of the hydroperoxo monoanion relative to the peroxo dianion.[6a,b] The conversion of **1** to **2** was reversible. Addition of excess NEt_3 to the solution of **2** instantly resulted in the near-quantitative regeneration of **1**, as shown by its characteristic absorption band. This cycle could be repeated several times [see Figure S1 in the Supporting Information (SI)]. These results further underscore that **2** is the conjugate acid of **1** and can be formulated as $[Fe^{III}(TMC)(OOH)]^{2+}$.

The Mössbauer samples of **1**—**3** contain large fractions of the designated complexes. In the spectrum of **1** shown in Figure 2A, ∼90% of the total Fe belongs to **1**; in Figure 2B, 80% of the Fe can be assigned to **2**, with 10% of the iron belonging to Fe^{IV}=O complex **3** (see below for analysis details). Analysis of a sample of **2** that was allowed to decay for 5 min after addition of $HClO_4$ showed that 90% of the total Fe corresponded to **3** (Figure S9). Thus, *the overall conversion of 1 to 3 is essentially quantitative.*

The electronic structures of **1** and **2** were established by EPR and Mössbauer spectroscopy. Both complexes are high-spin Fe^{III} with quite different zero-field splitting (ZFS) parameters and

Received: December 30, 2010
Published: April 25, 2011

dx.doi.org/10.1021/ja111742z | *J. Am. Chem. Soc.* 2011, 133, 7256–7259

Scheme 1. (A) TMC Ligand Used in This Study; (B) Conversion of 1 to 2 and Then to 3 via a Putative Short-Lived Fe^{V}=O Intermediate

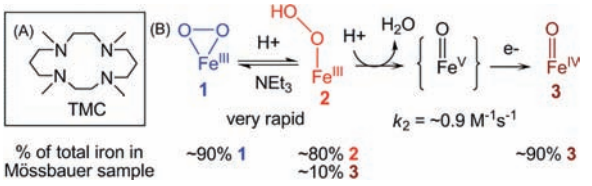

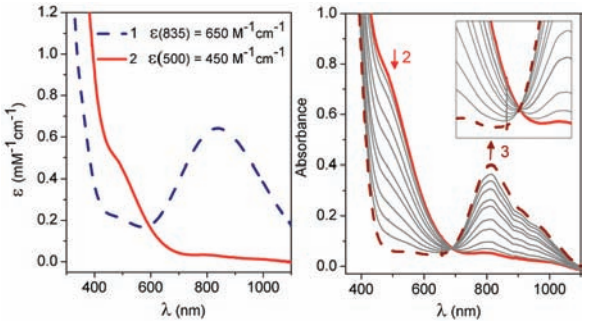

Figure 1. (left) UV−vis absorption spectra of $[Fe^{III}(TMC)(O_2)]^+$ (**1**) (blue dashed line) and $[Fe^{III}(TMC)(OOH)]^{2+}$ (**2**) (red solid line) in CH_3CN. (right) UV−vis absorption spectra during the conversion of **2** (red solid line) to $[Fe^{IV}(O)(TMC)(CH_3CN)]^{2+}$ (**3**) (brown dashed line) via the addition of ~20 equiv of $HClO_4$ in CH_3CN at −40 °C. b = 1 cm. Inset: Close-up view showing the isosbestic point at ~695 nm.

isomer shifts (Table S1). We analyzed the data with the $S = {}^5/_2$ spin Hamiltonian (eq 1):

$$\hat{H} = D(\hat{S}_z^2 - {}^{35}/_4) + E(\hat{S}_x^2 - \hat{S}_y^2) + \beta\hat{\mathbf{S}}\cdot\mathbf{g}\cdot\mathbf{B} + \hat{\mathbf{S}}\cdot\mathbf{A}\cdot\hat{\mathbf{I}} - g_n\beta_n\mathbf{B}\cdot\hat{\mathbf{I}} + \hat{H}_Q \quad (1)$$

where all symbols have their conventional meanings.

The X-band EPR spectrum of **1** exhibits, for the middle Kramers doublet, signals at g_{eff} = 4.58, 4.38, and ~4.1 (Figure 3A and Figures S4−S7). Mössbauer analysis (see the SI) showed that $D \approx -0.9$ cm^{-1} and $E/D = 0.28(1)$. With E/D fixed, the explanation of the EPR features of **1** required inclusion of substantial fourth-order ZFS parameters (eq 2):

$$\hat{H}_{4th} = \frac{F}{180}\left[35\hat{S}_z^4 - 30S(S+1)\hat{S}_z^2 + 25\hat{S}_z^2 - 6S(S+1) - 3S^2(S+1)^2\right] + \frac{a}{6}\left[\hat{S}_x^4 + \hat{S}_y^4 + \hat{S}_z^4 - \frac{1}{5}S(S+1)(3S^2+3S-1)\right] \quad (2)$$

For the simulation of Figure 2C, we used $F = -0.108$ cm^{-1} and $a = -0.017$ cm^{-1}. Large fourth-order parameters, namely, a = 0.074 cm^{-1} and F = 0.043 cm^{-1}, have been reported for Fe superoxide dismutase-azide,[10] together with D = 0.46 cm^{-1} and E/D = 0.255. An 8.0 T Mössbauer spectrum of **1** and a spectral simulation are shown in Figure 2A (see Figures S2 and S3 for additional spectra). The spectrum shown gives an isomer shift of δ = 0.58 mm/s for **1**, which is similar to that for the side-on peroxo complex $[Fe^{III}(N4Py)(\eta^2\text{-}O_2)]^+$ (δ = 0.61 mm/s).[6b] See the SI for additional details of the spectral analysis.

Analysis of the Mössbauer spectra of **2** shown in Figure 2B and Figure S8 yielded $D = +2.5$ cm^{-1}, $E/D = 0.097(7)$, and δ = 0.51 mm/s. The EPR spectrum of **2** (Figure 2D) exhibited signals at

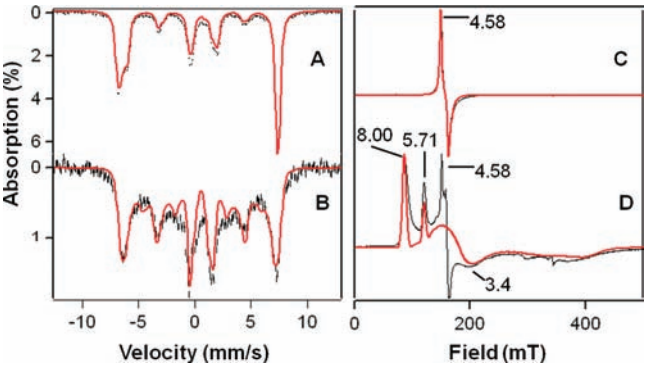

Figure 2. (left) 4.2 K Mössbauer spectra of **1** and **2** in 3:1 (v/v) PrCN/MeCN recorded in parallel applied fields (black lines) and simulations (red lines); parameters are given in Table S1. (A) 8.0 T spectrum of **1**. (B) 1.2 T spectrum of **2** after removing 10% due to **3** from the data. (right) X-band EPR spectra of **1** and **2** in 3:1 (v/v) PrCN/MeCN, shown as black lines. (C) Complex **1**. T = 15 K; microwave power = 0.02 mW; 1 mT modulation. The red line is a simulation using D = −0.91 cm^{-1}, E/D = 0.28, F = −0.108 cm^{-1} and a = −0.017 cm^{-1} (see the SI), **g** = (2.04, 1.98, 2.03), and distributed E/D with $\sigma_{E/D}$ = 0.038. (D) Complex **2**. T = 10 K; microwave power = 2.0 mW; 1 mT modulation. The red line is a simulation using D = 2.5 cm^{-1}, E/D = 0.097, **g** = (2.00, 2.00, 2.00), and $\sigma_{E/D}$ = 0.02. The sharp features at g_{eff} = 4.58 and 4.36 arise from residual **1** (representing 1% of the total Fe).

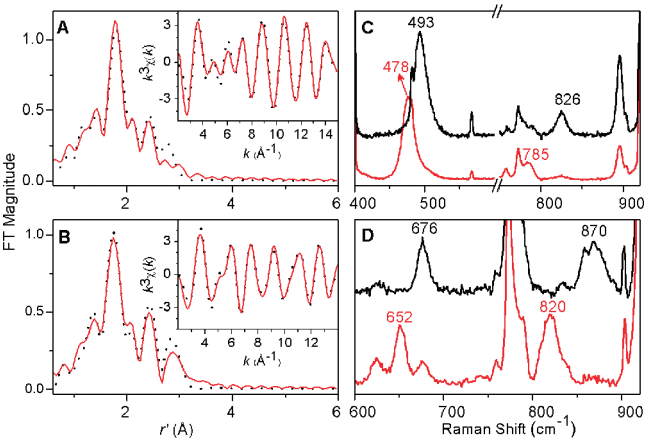

Figure 3. (left) Fits to the Fourier transforms of the Fe K-edge EXAFS data $[k^3\chi(k)]$ and (insets) Fourier-filtered EXAFS spectra $[k^3\chi(k)]$ for (A) **1** and (B) **2**. Experimental data are represented as black dotted lines, and fits are shown as red solid lines. Fits correspond to fits 9 for **1** (Table S2) and **2** (Table S3). (right) Resonance Raman spectra of (C) **1** and (D) **2** prepared with H_2O_2 (black line) or $H_2{}^{18}O_2$ (red line) (λ_{ex} = 647.1 nm for **1** and 514.5 nm for **2**).

g_{eff} = 8.00 (ground doublet), 5.71 (middle), and 3.4 (ground), consistent with the above D and E/D values. The parameters used for the simulations of **1** and **2** are listed in Table S1.

We also carried out Fe K-edge X-ray absorption spectroscopy (XAS) studies to obtain structural information and metric parameters for **1** and **2** (Figure 3A,B and Tables S1−S3). The EXAFS spectrum of **1** was best fit by two N/O scatterers at 1.93 Å and four N/O scatterers at 2.20 Å, while the best fit for **2** consisted of one N/O scatterer at 1.92 Å and four N/O scatterers at 2.15 Å. Interchanging the number of scatterers in the 1.9 Å subshells of **1** and **2**, which arise from the peroxo ligands, significantly worsened

dx.doi.org/10.1021/ja111742z |J. Am. Chem. Soc. 2011, 133, 7256–7259

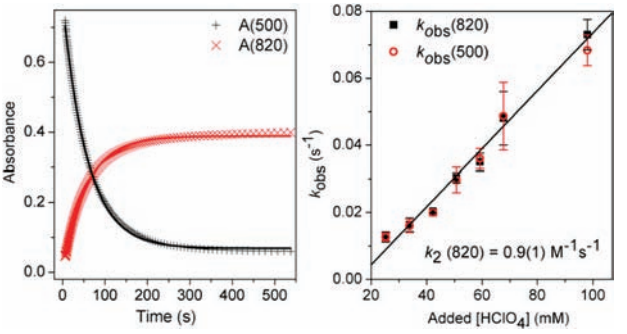

Figure 4. (left) Plots of absorbance at 500 and 820 nm vs time for the conversion of **2** to **3**. Solid lines represent fits of the reaction progress (absorbance at 500 and 820 nm) vs time to a typical first-order rate equation. Experimental conditions: 1.5 mM **2** and 34 mM $HClO_4$ in CH_3CN at −40 °C. (right) Plot of k_{obs}(820) and k_{obs}(500) vs added [$HClO_4$] for the conversion of **2** to **3**. Experimental conditions: 1.5 mM **2** in CH_3CN at −40 °C. The black line is a linear fit for k_{obs}(820). See the SI for additional experimental details.

the overall fit quality for both complexes, with unacceptable Debye−Waller factors for this subshell in both cases (Tables S2 and S3). These results led to the respective assignments of an η^2 binding mode for the dianionic peroxo ligand in **1** and an η^1 binding mode for the monoanionic hydroperoxo ligand in **2**. These assignments were supported by the observed 0.05 Å decrease in $r_{Fe-N_{TMC}}$ in going from **1** to **2**.[11]

Resonance Raman studies of **1** and **2** provided additional insight into how the difference in binding mode affects the two high-spin Fe^{III}−peroxo units. Resonance-enhanced vibrations were found for **1** at 826 and 493 cm^{-1} and for **2** at 870 and 676 cm^{-1} (Figure 3C,D and Figure S10). These features can be assigned respectively to ν(O−O) and ν(Fe−O) modes on the basis of the observed ^{18}O downshifts, which conformed to predictions for diatomic harmonic oscillators based on Hooke's law. The observed vibrational modes compare favorably to those for related complexes (Table S4). The sole exception is ν(Fe−O) for **2** at 676 cm^{-1}, which lies above the range of ν(Fe−O) values (420−620 cm^{-1}) found for other high-spin Fe^{III}−OOH complexes studied to date (Table S4). We speculate that the high ν(Fe−O) value for **2** may reflect the weaker electron-donating ability of the presumed CH_3CN ligand trans to the hydroperoxo unit relative to those for the other complexes. The stronger Fe−O bond suggested by the high ν(Fe−O) value for **2** is also likely to be an important factor that contributes to the observed cleavage of its O−O bond. In contrast, the Fe^{III}−OOH units of oxyhemerythrin[12] and SOR,[13] with ν(Fe−O) values that are at least 100 cm^{-1} smaller, undergo Fe−O bond cleavage in the course of their respective functions.

After its formation from **1**, **2** quickly decayed and underwent O−O bond cleavage to form $[Fe^{IV}(O)(TMC)(CH_3CN)]^{2+}$ (**3**)[14] in essentially quantitative yield (see above). The decay of **2** (monitored at 500 nm) occurred concomitantly with the appearance of **3** (monitored at 820 nm), with an isosbestic point at ∼695 nm (Figure 1 right). The time courses of the absorbance changes at both 500 and 820 nm could be fit with a simple first-order kinetic model (Figure 4 left), affording rate constants (k_{obs}) that were found to be identical within experimental error. The temperature dependence of the k_{obs} values was determined from −40 to −20 °C (Figure S11), giving rise to an Eyring plot that yielded the activation parameters $\Delta H^{\ddagger}$ = 44(2) kJ/mol and $\Delta S^{\ddagger}$ = −90(10) J mol^{-1} K^{-1}. These parameters are quite distinct from those determined for the reaction of $[Fe^{II}(TMC)(CH_3CN)]^{2+}$ with H_2O_2 in CH_3CN in the presence of 2,6-lutidine to form **3** [$\Delta H^{\ddagger}$ = 29(2) kJ/mol and $\Delta S^{\ddagger}$ = −144(10) J mol^{-1} K^{-1}], which involves a direct Fe^{II}/Fe^{IV}=O conversion.[15] On the other hand, the intermediacy of the Fe^{III}−OOH complex **2** has been postulated in the reactions of $[Fe^{II}(TMC)(NCCH_3)]^{2+}$ with O_2 in the presence of an H atom donor or its equivalent that afford **3** as the final product, but **2** has been elusive in these reactions.[8] Our results thus provide the first direct evidence to support this hypothesis.

This first unequivocal example of the conversion of a high-spin Fe^{III}−OOH species to an Fe^{IV}=O complex provides an opportunity to discern the factors that promote O−O bond cleavage in such species. Importantly, the conversion of **2** to **3** was found to be *proton-dependent*. As shown in the right panel of Figure 4, the values for both k_{obs}(500) and k_{obs}(820) increased linearly with added [$HClO_4$], and a second-order rate constant (k_2) of 0.9(1) M^{-1} s^{-1} at −40 °C was extracted from the slope of this plot. Also of significance is the observation that the quantitative yield of **3** from **1** was not affected even at the largest amounts of added acid, indicating that the added protons do not lead to Fe−O bond cleavage in **2** to release H_2O_2. The observed proton dependence of the formation of **3** strongly suggests that a proton promotes O−O bond cleavage.

Proton-assisted O−O bond cleavage has generally been associated with O−O bond heterolysis,[1,16,17] as protonation of the terminal oxygen atom of the Fe−OOH moiety converts hydroxide into a much better leaving group. Indeed, this is the generally accepted mechanism for the generation of the high-valent iron−oxo intermediate Compound I in heme enzymes.[1,16] Protons also promote the conversion of the peroxo intermediate of MMO into the corresponding diiron(IV) oxidant **Q**.[3] In model systems, it has been demonstrated that acid facilitates O−O bond heterolysis in the conversion of acylperoxoiron(III) porphyrin complexes to oxoiron(IV) porphyrin cation radical species.[17] Proton-assisted O−O bond heterolysis of Fe^{III}−OOH intermediates to generate Fe^{V}=O oxidants has also been proposed in the mechanisms of non-heme iron catalysts that use H_2O_2 as the oxidant to carry out C−H hydroxylation, C=C epoxidation and cis-dihydroxylation, and aromatic-ring hydroxylation.[18] The fact that many of the oxidations are highly stereoselective argues against the involvement of HO· species that would be produced from O−O bond homolysis.[18a] Indeed, an EPR signal assigned to the putative Fe^{V} oxidant has been reported.[19] On the other hand, DFT calculations by Solomon[5] revealed a very significant barrier for O−O bond homolysis of high-spin Fe^{III}−OOH(R) species. Taken together, the points presented above and our observed proton dependence for the conversion of **2** into **3** lead us to favor a heterolytic cleavage mechanism that would initially afford a formally Fe^{V}=O species. Unfortunately, our attempts to intercept the putative Fe^{V}=O species have not been successful. Because of the neutral nature of the TMC ligand, it is perhaps not surprising that the putative $[Fe^{V}(O)(TMC)]^{3+}$ species has such a short lifetime; it could be rapidly reduced by one of several possible reductants present in the reaction mixture (e.g., H_2O_2, NEt_3, or even the CH_3CN solvent) to afford **3**, which was experimentally observed (Scheme 1B). Indeed, the only well-characterized Fe^{V}=O complex reported to date is supported by a tetraanionic macrocyclic ligand that significantly extends the lifetime of the Fe^{V}=O unit.[20]

dx.doi.org/10.1021/ja111742z |*J. Am. Chem. Soc.* 2011, 133, 7256–7259

In summary, we have reported here the first example of a synthetic high-spin Fe^{III}—OOH complex that is quantitatively converted to an oxoiron(IV) complex via O—O bond cleavage. This transformation is promoted by two factors: (a) the strong Fe—O bond found for **2** (as indicated by its high Raman frequency), which appears to prevent Fe—O bond scission even in the presence of 0.1 M $HClO_4$, and (b) the key role of protons. Irrespective of the precise nature of the cleavage mechanism, the conversion of **2** to **3** demonstrates that O—O bond cleavage can indeed occur readily at a high-spin Fe^{III} center, even at −40 °C. This example thus serves as a synthetic precedent for the proton-assisted conversion of high-spin Fe^{III}—OOH intermediates to high-valent iron—oxo oxidants in the proposed mechanisms of dioxygen-activating non-heme enzymes such as the cis-dihydroxylating Rieske dioxygenases[2] and bacterial multicomponent monooxygenases such as MMO[3] and toluene monooxygenase.[21]

■ ASSOCIATED CONTENT

Supporting Information. Detailed experimental procedures and physical methods, a plot for the interconversion between **1** and **2**, a more extensive discussion of the Mössbauer and EPR simulations of **1** and **2**, details of the EXAFS analysis, and an Eyring plot for conversion of **2** to **3**. This material is available free of charge via the Internet at http://pubs.acs.org.

■ AUTHOR INFORMATION

Corresponding Author
emunck@cmu.edu; larryque@umn.edu

■ ACKNOWLEDGMENT

Support was provided by NIH Grants GM-33162 (L.Q.), GM-38767 (L.Q.), and EB-001475 (E.M.); NIH Postdoctoral Fellowships ES017390 (M.A.C.) and GM093479 (K.M.V.H.); and a University of Minnesota Doctoral Dissertation Fellowship (F.L.). XAS data were collected at Beamline 7-3 of the Stanford Synchrotron Radiation Lightsource, which was supported by the U.S. Department of Energy and the National Institutes of Health. We thank Dr. Erik R. Farquhar and Dr. Jason England for insightful discussions.

■ REFERENCES

(1) (a) Denisov, I. G.; Makris, T. M.; Sligar, S. G.; Schlichting, I. *Chem. Rev.* **2005**, *105*, 2253. (b) Sligar, S. G.; Makris, T. M.; Denisov, I. G. *Biochem. Biophys. Res. Commun.* **2005**, *338*, 346. (c) Watanabe, Y.; Nakajima, H.; Ueno, T. *Acc. Chem. Res.* **2007**, *40*, 554.

(2) (a) Kovaleva, E. G.; Neibergall, M. B.; Chakrabarty, S.; Lipscomb, J. D. *Acc. Chem. Res.* **2007**, *40*, 475. (b) Neibergall, M. B.; Stubna, A.; Mekmouche, Y.; Münck, E.; Lipscomb, J. D. *Biochemistry* **2007**, *46*, 8004.

(3) (a) Lee, S.-K.; Lipscomb, J. D. *Biochemistry* **1999**, *38*, 4423. (b) Tinberg, C. E.; Lippard, S. J. *Biochemistry* **2009**, *48*, 2145.

(4) (a) Kurtz, D. M., Jr. *J. Inorg. Biochem.* **2006**, *100*, 679. (b) Kovacs, J. A.; Brines, L. M. *Acc. Chem. Res.* **2007**, *40*, 501.

(5) (a) Solomon, E. I.; Decker, A.; Lehnert, N. *Proc. Natl. Acad. Sci. U.S.A.* **2003**, *100*, 3589. (b) Lehnert, N.; Ho, R. Y. N.; Que, L., Jr.; Solomon, E. I. *J. Am. Chem. Soc.* **2001**, *123*, 12802.

(6) Low-spin Fe^{III}—OOH complexes: (a) Simaan, A. J.; Döpner, S.; Banse, F.; Bourcier, S.; Bouchoux, G.; Boussac, A.; Hildebrandt, P.; Girerd, J.-J. *Eur. J. Inorg. Chem.* **2000**, 1627. (b) Roelfes, G.; Vrajmasu, V.; Chen, K.; Ho, R. Y. N.; Rohde, J.-U.; Zondervan, C.; la Crois, R. M.; Schudde, E. P.; Lutz, M.; Spek, A. L.; Hage, R.; Feringa, B. L.; Münck, E.; Que, L., Jr. *Inorg. Chem.* **2003**, *42*, 2639. (c) Mairata i Payeras, A.; Ho, R. Y. N.; Fujita, M.; Que, L., Jr. *Chem.—Eur. J.* **2004**, *10*, 4944. (d) Shearer, J.; Scarrow, R. C.; Kovacs, J. A. *J. Am. Chem. Soc.* **2002**, *124*, 11709.

(7) High-spin Fe^{III}—OOH complexes: (a) Wada, A.; Ogo, S.; Nagatomo, S.; Kitagawa, T.; Watanabe, Y.; Jitsukawa, K.; Masuda, H. *Inorg. Chem.* **2002**, *41*, 616. (b) Kitagawa, T.; Dey, A.; Lugo-Mas, P.; Benedict, J. B.; Kaminsky, W.; Solomon, E.; Kovacs, J. A. *J. Am. Chem. Soc.* **2006**, *128*, 14448.

(8) (a) Kim, S. O.; Sastri, C. V.; Seo, M. S.; Kim, J.; Nam, W. *J. Am. Chem. Soc.* **2005**, *127*, 4178. (b) Thibon, A.; England, J.; Martinho, M.; Young, V. G.; Frisch, J. R.; Guillot, R.; Girerd, J.-J.; Münck, E.; Que, L., Jr.; Banse, F. *Angew. Chem., Int. Ed.* **2008**, *47*, 7064. (c) Hong, S.; Lee, Y.-M.; Shin, W.; Fukuzumi, S.; Nam, W. *J. Am. Chem. Soc.* **2009**, *131*, 13910. (d) Lee, Y.-M.; Hong, S.; Morimoto, Y.; Shin, W.; Fukuzumi, S.; Nam, W. *J. Am. Chem. Soc.* **2010**, *132*, 10668.

(9) Annaraj, J.; Suh, Y.; Seo, M. S.; Kim, S. O.; Nam, W. *Chem. Commun.* **2005**, 4529.

(10) Schmidt, M.; Scherk, C.; Iakovleva, O.; Nolting, H. F.; Meier, B.; Parak, F. *Inorg. Chim. Acta* **1998**, *275*, 65.

(11) The high-spin state for **2** results from constraints imposed by the TMC macrocycle that prevent formation of the shorter Fe—N bonds required for a low-spin Fe^{III} center.

(12) (a) Brunold, T. C.; Solomon, E. I. *J. Am. Chem. Soc.* **1999**, *121*, 8277. (b) Shiemke, A. J.; Loehr, T. M.; Sanders-Loehr, J. *J. Am. Chem. Soc.* **1984**, *106*, 4951.

(13) Katona, G.; Carpentier, P.; Nivière, V.; Amara, P.; Adam, V.; Ohana, J.; Tsanov, N.; Bourgeois, D. *Science* **2007**, *316*, 449.

(14) Rohde, J.-U.; In, J.-H.; Lim, M. H.; Brennessel, W. W.; Bukowski, M. R.; Stubna, A.; Münck, E.; Nam, W.; Que, L., Jr. *Science* **2003**, *299*, 1037.

(15) Li, F.; England, J.; Que, L., Jr. *J. Am. Chem. Soc.* **2010**, *132*, 2134.

(16) (a) Aikens, J.; Sligar, S. G. *J. Am. Chem. Soc.* **1994**, *116*, 1143. (b) Dunford, H. B.; Hewson, W. D.; Steiner, H. *Can. J. Chem.* **1978**, *56*, 2844.

(17) Groves, J. T.; Watanabe, Y. *J. Am. Chem. Soc.* **1988**, *110*, 8443.

(18) (a) Chen, K.; Costas, M.; Kim, J.; Tipton, A. K.; Que, L., Jr. *J. Am. Chem. Soc.* **2002**, *124*, 3026. (b) Mas-Ballesté, R.; Que, L., Jr. *J. Am. Chem. Soc.* **2007**, *129*, 15964. (c) Chen, M. S.; White, M. C. *Science* **2007**, *318*, 783. (d) Makhlynets, O. V.; Das, P.; Taktak, S.; Flook, M.; Mas-Ballesté, R.; Rybak-Akimova, E. V.; Que, L., Jr. *Chem.—Eur. J.* **2009**, *15*, 13171. (e) Joon, Y.; Wilson, S. A.; Jang, Y. K.; Seo, M. S.; Nehru, K.; Hedman, B.; Hodgson, K. O.; Bill, E.; Solomon, E. I.; Nam, W. *Angew. Chem., Int. Ed.* **2009**, *48*, 1257. (f) Das, P.; Que, L., Jr. *Inorg. Chem.* **2010**, *49*, 9479. (g) Makhlynets, O. V.; Rybak-Akimova, E. V. *Chem.—Eur. J.* **2010**, *16*, 13995.

(19) Lyakin, O. Y.; Bryliakov, K. P.; Britovsek, G. J. P.; Talsi, E. P. *J. Am. Chem. Soc.* **2009**, *131*, 10798.

(20) Tiago de Oliveira, F.; Chanda, A.; Banerjee, D.; Shan, X.; Mondal, S.; Que, L., Jr.; Bominaar, E. L.; Münck, E.; Collins, T. J. *Science* **2007**, *315*, 835.

(21) Song, W. J.; McCormick, M. S.; Behan, R. K.; Sazinsky, M. H.; Jiang, W.; Lin, J.; Krebs, C.; Lippard, S. J. *J. Am. Chem. Soc.* **2010**, *132*, 13582.